JOURNAL OF AIRCRAFT
Vol. 42, No. 4, July–August 2005

Aeroelastic Calculations for the Hawk Aircraft Using the Euler Equations

M. A. Woodgate,* K. J. Badcock,† A. M. Rampurawala,‡ and B. E. Richards§
University of Glasgow, Glasgow, Scotland G12 8QQ, United Kingdom
and
D. Nardini¶ and M. J. deC Henshaw**
BAE SYSTEMS, Brough, England HU15 1EQ, United Kingdom

This paper demonstrates coupled time-domain computational-fluid-dynamics (CFD) and computational-structural-dynamics simulations for flutter analysis of a real aircraft in the transonic regime. It is shown that a major consideration for a certain class of structural models is the transformation method, which is used to pass information between the fluid and structural grids. The aircraft used for the calculations is the BAE Systems Hawk. A structural model, which has been developed by BAE Systems for simplified linear flutter calculations, only has a requirement for $\mathcal{O}(10)$ degrees of freedom. There is a significant mismatch between this and the surface grid on which loads and deflections are defined in the CFD calculation. This paper extends the constant volume tetrahedron tranformation, previously demonstrated for wing-only aeroelastic calculations, to multicomponent, or full aircraft, cases and demonstrates this for the Hawk. A comparison is made with the predictions of a linear flutter code.

Nomenclature

$\boldsymbol{a}, \boldsymbol{b}, \boldsymbol{c}, \boldsymbol{d}$	=	vectors used to define constant-volume-tetrahedron (CVT) transformation
d	=	magnitude of vector $\boldsymbol{d}$
E	=	fluid total energy
$\boldsymbol{F}, \boldsymbol{G}, \boldsymbol{H}$	=	convective flux vectors
$\boldsymbol{f}$	=	force acting at the grid points
$\boldsymbol{K}$	=	structural stiffness matrix
$\boldsymbol{M}$	=	structural mass matrix
p	=	fluid pressure
t	=	real time
U, V, W	=	contravariant Cartesian fluid velocity components
u, v, w	=	Cartesian fluid velocity components
$\boldsymbol{W}$	=	vector of conserved fluid variables
x, y, z	=	Cartesian coordinates
$\boldsymbol{x}$	=	grid locations
x_t, y_t, z_t	=	fluid grid speeds
α, β	=	in-plane coordinates in CVT transformation
γ	=	out-plane coordinate in CVT transformation
δ	=	change in grid locations
η	=	generalized modal coordinates
ρ	=	fluid density
ϕ	=	mode shape
ψ_i^0	=	blending function for transfinite interpolation
ω	=	modal frequency
$\triangle$	=	triangle formed from the structural grid points

Subscripts

a	=	aerodynamic surface grid
s	=	structural grid

Superscript

n	=	time level

Introduction

THE demonstration of aeroelastic stability is a key part of the aircraft design and qualification process. Linear methods are the standard industry analysis tool, backed up by extensive flight testing. It is well known that linear theories, based on potential flow models, cannot give good predictions of aerodynamics in the transonic regime in which civil and military aircraft often fly. Potentially, computational fluid dynamics (CFD) is a powerful tool for transonic flows, and in recent years convincing demonstrations of the predictions of both steady and unsteady flows have been made for many complex configurations.

Coupled CFD/computational-structural-dynamics (CSD) calculations have become increasingly common in recent years, driving developments in grid movement (e.g., Refs. 1 and 2), geometric conservation laws,[3] solution sequencing in time,[4] and intergrid transformation of data.[5–7] The latter problem, especially for structural models that feature simplified geometric representations, can be a delicate matter, as shown for some wing responses in Goura et al.[8]

The routine solution of complete aircraft problems is essential for coupled simulations to start making a significant impact on industrial practice. There are several examples discussed in the literature. The computational aeroelastic programme-transonic small disturbance code was used to investigate residual pitch oscillations experienced by the B2 stealth bomber. The convincing analysis showed that these were caused by a low-frequency shock-wave motion on the wing (see Dreim et al.[9]), something that linear analysis had inevitably missed. Because of the level of modelling used, both the structural and aerodynamic grids were defined on plates, and hence well-established methods from linear analysis could be used to transfer information between the grids.

Some recent examples based on the Euler or Reynolds-averaged Navier–Stokes (RANS) models have been motivated by store-induced limit-cycle oscillation behavior for the F-16 aircraft. Melville[10] solved a RANS model on a structured grid, with

Received 4 October 2003; revision received 15 July 2004; accepted for publication 15 July 2004.

*Research Assistant, Computational Fluid Dynamics Laboratory, Department of Aerospace Engineering.
†Reader, Computational Fluid Dynamics Laboratory, Department of Aerospace Engineering; gnaa36@aero.gla.ac.uk.
‡Ph.D. Student, Computational Fluid Dynamics Laboratory, Department of Aerospace Engineering.
§Mechan Professor, Computational Fluid Dynamics Laboratory, Department of Aerospace Engineering. Associate Fellow AIAA.
¶Aerodynamics Engineer, Aerodynamic Technology.
**Senior Specialist, Aerodynamic Technology.

a simplified structural description, to simulate this problem. A transformation based on a component-wise method was used, which forced components to remain attached at junctions. Farhat et al.[11] simplified the transfer of information, for the F-16 problem, by defining both grids on the same surface and using an unstructured, Euler CFD solver and a detailed structural model. Finally, simulations by Pranata et al.[12] used a block structured grid and a simplified structural model to simulate the same problem, with transformation being done by volume splines. In all cases at least qualitatively correct behavior was obtained, but it is difficult to assess the precision of the simulations caused by a lack of suitable data with which to compare and to the cost of making detailed grid and time-refinement studies.

This paper builds on previous work by the authors that has demonstrated time-domain aeroelastic analysis of wings. Particular attention has been paid to the issue of transferring information between simplified structural models and CFD surface grids. A simple method to achieve this, called the constant-volume-tetrahedron (CVT) transformation was proposed in Goura.[13] This was then extended to multicomponent configurations by Badcock et al.[14] The current paper demonstrates the method for the time-marching aeroelastic analysis of a real aircraft.

The Hawk family of aircraft, manufactured by BAE Systems, first entered service with the Royal Air Force in 1976. A stick model that has been built up by the company using ground-resonance-test data provides a finite element structural model that can be used for linear flutter calculations. This provides a model with a small number of degrees of freedom that can realistically reproduce the frequency, mode shapes, and damping of the aircraft. The use of low-order models is desirable because every possible configuration of stores must be considered. The number of cases can run into the thousands, and even at a few minutes per configuration a complete analysis can take weeks to perform. The symmetric modes have been observed from linear analysis to be the most critical for exhibiting instability.

The current paper continues with a description of the CFD, CSD, and time-marching formulations. Then, the transfer of information between the structural and fluid surface grids is considered. Because of the sparseness of this particular structural grid, this turns out to be problematic. Finally, time-domain results based on the Euler equations are presented.

Formulation

Flow Solver

The three-dimensional Euler equations can be written in nondimensional conservative form as

$$\frac{\partial \boldsymbol{W}}{\partial t} + \frac{\partial \boldsymbol{F}}{\partial x} + \frac{\partial \boldsymbol{G}}{\partial y} + \frac{\partial \boldsymbol{H}}{\partial z} = 0 \tag{1}$$

The flux vectors $\boldsymbol{F}$, $\boldsymbol{G}$, and $\boldsymbol{H}$ are

$$\boldsymbol{F} = \begin{pmatrix} \rho U \\ \rho u U + p \\ \rho v U \\ \rho w U \\ U(\rho E + p) + x_t p \end{pmatrix}, \qquad \boldsymbol{G} = \begin{pmatrix} \rho V \\ \rho u V \\ \rho v V + p \\ \rho w V \\ V(\rho E + p) + y_t p \end{pmatrix}$$

$$\boldsymbol{H} = \begin{pmatrix} \rho W \\ \rho u W + p \\ \rho v W \\ \rho w W + p \\ W(\rho E + p) + z_t p \end{pmatrix}$$

The terms U, V, and W are the contravariant velocities defined by

$$U = u - x_t, \qquad V = v - y_t, \qquad W = w - z_t \tag{2}$$

where x_t, y_t, and z_t are the grid speeds in the Cartesian directions.

The Euler equations are discretized on curvilinear multiblock body-conforming grids using a cell-centered finite volume method, which converts the partial differential equations of (1) into a set of ordinary differential equations. The convective terms are discretized using Osher's[15] upwind method. Monotone Upwind Scheme for Conservation Laws (MUSCL) variable extrapolation (see Van Leer[16]) is used to provide second-order accuracy with the Van Albada limiter to prevent spurious oscillations around shock waves. Following Jameson,[17] the spatial residual is modified by adding a second-order discretization of the real-time derivative to obtain a modified steady-state problem for the flow solution at the next real-time step, which is solved through pseudotime. This pseudotime problem is solved using an unfactored implicit method, based on an approximate linearization of the residual. The linear system is solved in unfactored form using a Krylov subspace method with block incomplete upper lower preconditioning. The preconditioner is decoupled between blocks to allow a very high efficiency on parallel computers with little detriment to the convergence of the linear solver. For the Jacobian matrix of the CFD residual function, approximations that reduce the size and improve the conditioning of the linear system without compromising the stability of the time marching are made.

The geometries of interest deform during the motion, and the mesh must be moved to conform with the evolving geometry. This is achieved using transfinite interpolation of displacements within the blocks containing the aircraft. More elaborate treatments that move blocks to maintain grid orthogonality are possible, as in Tsai et al.,[1] but are not necessary here because only small deflections are encountered. The surface deflections are interpolated to the volume grid points $\boldsymbol{x}_{ijk}$ as

$$\delta \boldsymbol{x}_{ijk} = \psi_j^0 \delta \boldsymbol{x}_{a,ik} \tag{3}$$

where ψ_j^0 are values of a blending function (see Gordon and Hall[18]), which varies between one at the aircraft surface and zero at the block face opposite. The surface deflections $\boldsymbol{x}_{a,ik}$ are obtained from the transformation of the deflections on the structural grid and so ultimately depend on the values of the generalized structural coordinate η_i (defined next). The grid speeds can be obtained by differentiating Eq. (3) to obtain their explicit dependence on the values of $\dot{\eta}_i$.

This formulation is implemented in the Glasgow University flow code Parallel Multiblock. This solves the Euler (and RANS) equations on block structured grids. A wide variety of unsteady flow problems, including cavity flows, aerospike flows, delta-wing aerodynamics, rotorcraft problems, and transonic buffet have been studied using this code. More details on the flow solver can be found in Badcock et al.[19]

Structural Solver

Finite element methods allow for the static and dynamic response of a structure to be determined. Stiffness $\boldsymbol{K}$ and mass $\boldsymbol{M}$ matrices are used to determine the equation of motion of an elastic structure subjected to an external force $\boldsymbol{f}_s$ as

$$\boldsymbol{M}\delta\ddot{\boldsymbol{x}}_s + \boldsymbol{K}\delta\boldsymbol{x}_s = \boldsymbol{f}_s \tag{4}$$

where $\delta\boldsymbol{x}_s$ is a vector of displacements on a grid of points $\boldsymbol{x}_s$. Because the structural system under consideration is assumed to be linear, its characteristics are determined once and for all prior to making the flutter calculations, so that $\boldsymbol{M}$ and $\boldsymbol{K}$ are constant matrices generated, in this case, by the commercial package MSC/NASTRAN.

The aircraft deflections $\delta\boldsymbol{x}_s$ are defined at a set of grid points $\boldsymbol{x}_s$ by

$$\delta\boldsymbol{x}_s = \sum \eta_i \phi_i \tag{5}$$

where ϕ_i are the mode shapes and η_i the generalized displacements. Here the η_i depend on time, but the mode shapes do not. The values of ϕ_i and ω_i are calculated by solving the eigenvalue problem

$$\left[\boldsymbol{M} - \omega_i^2 \boldsymbol{K}\right]\phi_i = 0 \tag{6}$$

The eigenvectors are scaled so that

$$[\phi_i]^T \boldsymbol{M} [\phi_i] = 1 \tag{7}$$

Projecting the finite element equations onto the mode shapes results in the equations

$$\frac{\mathrm{d}^2\eta_i}{\mathrm{d}t^2} + \omega_i^2\eta_i = \phi_i^T \boldsymbol{f}_s \tag{8}$$

where $\boldsymbol{f}_s$ is the vector of external forces at the structural grid points. This equation can be solved by a two-stage Runge–Kutta method, which requires a knowledge of $\boldsymbol{f}_s^n$ and $\boldsymbol{f}_s^{n+1}$. To avoid introducing sequencing errors by approximating the term $\boldsymbol{f}_s^{n+1}$, the Runge–Kutta solution is iterated in pseudotime along with the fluid solution, that is, the latest estimate for $\boldsymbol{f}_s^{n+1}$ is used in the Runge–Kutta solution. At convergence of the pseudotime iterations, the structural and fluid solutions are properly sequenced in time. The cost of the coupled calculation resides with the CFD solver when modal structural models are used. The CFD solver used in the current work is of good efficiency in the sense that the time step is always chosen to adequately resolve the solution temporally and is never chosen to facilitate the operation of the solver caused by stability or any other numerical considerations. It is our experience that building the structural solution into the pseudotime loop does nothing to change the performance of the flow solver, and there would be nothing to gain, for this CFD solver, from using, for example, the family of staggered schemes,[4] as we have shown for the AGARD wing test case in Goura et al.[20]

Finally, the structural models used for flutter prediction by industry usually have geometric simplifications, such as representing the wings as plates or the fuselage as a beam. There is a good case, especially as the modes have been derived from a finite element model, for using a detailed structural model for CFD–CSD simulations. This resolves a number of questions introduced by the use of simplified models and sits more comfortably with the desire to carry out high-fidelity simulations. However, there is a need for consistency of models across the range of methods used in flutter analysis, and legacy models (such as the one used here) will continue to be used. It is therefore necessary to use these simplified models for demonstration calculations of CFD-based aeroelastic analysis. A complementary research activity (e.g., Lucia et al.[21]) aims to derive reduced-order aerodynamic models for transonic analysis, in which case a change to detailed structural models is not necessarily appropriate. It is the authors' opinion that simplified structural models will be in use for some time to come and that CFD-based analysis methods must be able to cope with the problems introduced thereby.

Linear Methods

The doublet-lattice method (DLM) is a method for modeling the aerodynamics of oscillating lifting surfaces that reduces to the vortex-lattice method at zero reduced frequency. Based on potential flow theory, the DLM cannot describe nonlinear transonic or viscous aerodynamic effects. Industry flutter analysis tends to use the DLM (this is the case for the Hawk), and the linear predictions have been used successfully as part of an overall process for predicting flutter, despite the theoretical limitations. They therefore provide an essential point of reference for more sophisticated methods, such as those based on the Euler equations for aerodynamic modeling. Linear flutter speeds for the test case used in this paper have been derived using MSC/NASTRAN with DLM aerodynamic modeling.

The MSC/NASTRAN aerodynamic model includes the influence of the wing, tailplane, and rudder. However, because these lifting surfaces are represented as having no thickness and the modes are symmetric, the rudder does not effect the results. The fuselage is not included in the aerodynamic model. The wing has the fairing removed, and the dihedral angles of the wing and tailplane are modeled in the DLM but not the angle of incidence of the wing.

Transformation Methods

The complexity of achieving effective information transfer between the structural and fluid grids is often underestimated. The coupled solver needs to determine accurately the displacement of the fluid grid points $\delta\boldsymbol{x}_a$ based on the deflections of the structural grid points $\delta\boldsymbol{x}_s$. These latter are caused by the fluid forces on the structural grid points $\boldsymbol{f}_s$, which must be accurately determined from the known forces on the fluid surface grid points $\boldsymbol{f}_a$. One technique used in American industry is described in Brown.[5] The two grids are not, in general, coincident, and where CFD is used to derive the aerodynamic forces it is likely that the grids will have no common interface, as is the case for the Hawk example considered here.

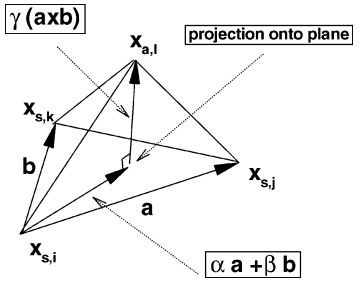

Fig. 1 Tetrahedron used for the CVT transformation.

The CVT scheme is a transformation technique proposed in Goura.[13] Each fluid surface grid point $\boldsymbol{x}_{a,l}$ is first associated with a triangular element $\triangle$ constructed from three structural grid points $\boldsymbol{x}_{s,i}$, $\boldsymbol{x}_{s,j}$, and $\boldsymbol{x}_{s,k}$. The position of $\boldsymbol{x}_{a,l}$ is given by the expression

$$\boldsymbol{x}_{a,l} - \boldsymbol{x}_{s,i}(t) = \alpha\boldsymbol{a} + \beta\boldsymbol{b} + \gamma\boldsymbol{d} \tag{9}$$

where $\boldsymbol{a} = \boldsymbol{x}_{s,j} - \boldsymbol{x}_{s,i}$, $\boldsymbol{b} = \boldsymbol{x}_{s,k} - \boldsymbol{x}_{s,i}$, and $\boldsymbol{d} = \boldsymbol{a} \times \boldsymbol{b}$. Here the term $\alpha\boldsymbol{a} + \beta\boldsymbol{b}$ represents the location of the projection of $\boldsymbol{x}_{a,l}$ onto $\triangle$, and $\gamma\boldsymbol{d}$ is the component out of the plane of $\triangle$, as shown in Fig. 1. In the preceding the values of α, β, and γ are calculated as

$$\alpha = \frac{|\boldsymbol{b}|^2(\boldsymbol{a}.\boldsymbol{c}) - (\boldsymbol{a}.\boldsymbol{b})(\boldsymbol{b}.\boldsymbol{c})}{|\boldsymbol{a}|^2|\boldsymbol{b}|^2 - (\boldsymbol{a}.\boldsymbol{b})(\boldsymbol{a}.\boldsymbol{b})} \tag{10}$$

$$\beta = \frac{|\boldsymbol{a}|^2(\boldsymbol{b}.\boldsymbol{c}) - (\boldsymbol{a}.\boldsymbol{b})(\boldsymbol{a}.\boldsymbol{c})}{|\boldsymbol{a}|^2|\boldsymbol{b}|^2 - (\boldsymbol{a}.\boldsymbol{b})(\boldsymbol{a}.\boldsymbol{b})} \tag{11}$$

$$\gamma = \frac{(\boldsymbol{c}.\boldsymbol{d})}{|\boldsymbol{d}|^2} \tag{12}$$

Equation (9) gives a nonlinear relationship between the fluid and structural locations, which can be linearized in the structural displacements to give

$$\delta\boldsymbol{x}_{a,l} = \boldsymbol{A}\delta\boldsymbol{x}_{s,i} + \boldsymbol{B}\delta\boldsymbol{x}_{s,j} + \boldsymbol{C}\delta\boldsymbol{x}_{s,k} \tag{13}$$

$$\boldsymbol{A} = \boldsymbol{I} - \boldsymbol{B} - \boldsymbol{C}, \qquad \boldsymbol{B} = \alpha I - \gamma\mathcal{U}\mathcal{V}(\boldsymbol{b})$$

$$\boldsymbol{C} = \beta I + \gamma\mathcal{U}\mathcal{V}(\boldsymbol{a}), \qquad \mathcal{U} = I - (2/d^2)\mathcal{D}(\boldsymbol{d})\mathcal{S}(\boldsymbol{d}) \tag{14}$$

$$\mathcal{V}(\boldsymbol{z}) = \begin{pmatrix} 0 & -z_3 & z_2 \\ z_3 & 0 & -z_1 \\ -z_2 & z_1 & 0 \end{pmatrix} \tag{15}$$

$$\mathcal{D}(\boldsymbol{z}) = \begin{pmatrix} z_1 & 0 & 0 \\ 0 & z_2 & 0 \\ 0 & 0 & z_3 \end{pmatrix} \tag{16}$$

$$\mathcal{S}(\boldsymbol{z}) = \begin{pmatrix} z_1 & z_2 & z_3 \\ z_1 & z_2 & z_3 \\ z_1 & z_2 & z_3 \end{pmatrix} \tag{17}$$

To avoid incurring significant errors from this linearization, it is always applied about the current structural location, as opposed to the original (undeflected) one. Hence there is a linear relationship for each application of the transformation, and the principle of virtual work is then used to give the force transformation. Denoting the linear relationship defined by Eq. (13) as

$$\delta\boldsymbol{x}_a = S(\boldsymbol{x}_a, \boldsymbol{x}_s)\delta\boldsymbol{x}_s \tag{18}$$

the force transformation is given as

$$\delta\boldsymbol{f}_s = S^T\delta\boldsymbol{f}_a \tag{19}$$

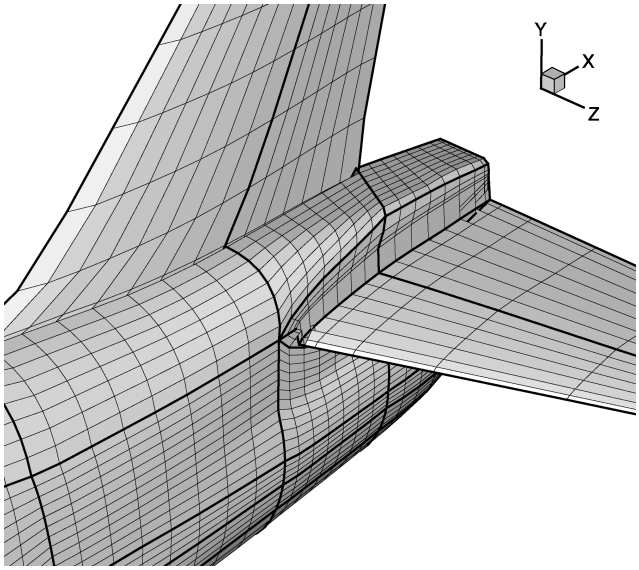

a) One level

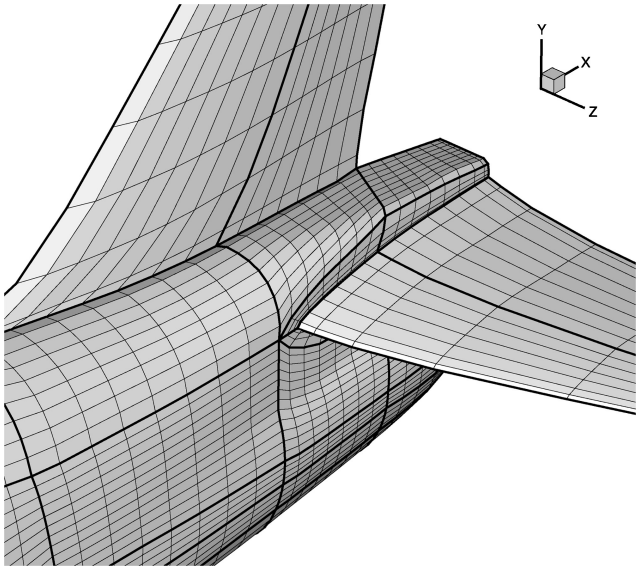

b) Two levels

Fig. 2 Difference in one and two levels transformed surfaces showing the folding of the grid in the junction regions when using the one level transformation.

This method was used for single component aeroelastic calculations in Goura[13] and Goura et al.[6] A version of this method that deals with structural models that feature beams was developed in Badcock et al.[14]

For complete aircraft cases, problems arise at junctions when the method is applied component-wise. In particular, gaps can appear because there is no guarantee that a point lying on a junction will be identically transformed for the two components meeting at the junction. This is illustrated in Fig. 2a, where the tailplane and fuselage junction become crossed over and the vertical fin detaches from the fuselage. Even very small mismatches like this can lead to poor grid quality (see Badcock et al.[14]).

To overcome this, a multilevel mapping is used. The idea is that the motion of points on, for example, the wing is not independent of the fuselage to which the wing is attached. The wing points must therefore attach to the fuselage as the wing root is approached. A transformation is defined for each component and is then averaged according to a hierachy to ensure that components match at junctions. In the current case two levels are defined, one for the fuselage and one for all other components. The fuselage is defined as being predominant so that all components attach to the fuselage as it is approached. The distance from the nearest fuselage fluid point is calculated for all fluid surface points. This is then used to weight the transformations obtained from the two levels, one based on linking all components to a triangle on the fuselage structural grid and the other based on linking to a triangle on the correct component (i.e., wing fluid points to triangles on the wing structural grid, fuselage fluid points to the fuselage structural points, etc.). As the fuselage is approached, all of the weight is put on the fuselage-based transformation, ensuring that the junctions are properly defined. The resulting improvements in the surface definition are shown in Fig. 2b.

The coarsest triangulation of the Hawk structural model leads to only 78 elements as shown in Fig. 3. The lack of stuctural elements means that the method used to associate fluid points with a triangle $\triangle$ becomes critical. This mapping is done as a preprocessing step and is the only input required for the time-marching calculation. The method used previously in Goura[13] and Badcock et al.[14] was to select the triangle that minimizes the distance between the projection of the fluid point and the centroid of the structural triangles. This works well when the structural grid is finer than in the current case. However, on coarse structural grids the situation shown in Fig. 4 arises. The line P_1P_2 shows the transition between $\triangle_{\mathrm{ABD}}$ and $\triangle_{\mathrm{BCD}}$ when nearest centroids are used. This method of association means extrapolation is used, for example, near corner D of $\triangle_{\mathrm{ABD}}$ when it is preferable to use linear interpolation within triangle $\triangle_{\mathrm{ABD}}$. To keep extrapolation to a minimum, the following straightforward modification was made.

For each triangle in the structural model, we calculate the area of the jth triangle ABC and the sum of the areas of triangles APB, BPC, and APC, where P is the projected point $\boldsymbol{x}_{p,i}$, as shown in Fig. 5. The difference in the sum of the three triangles containing the projected point and the original triangle is defined as

$$X_{\triangle_j} = |\triangle_{\mathrm{ABC}} - \triangle_{\mathrm{APB}} - \triangle_{\mathrm{BPC}} - \triangle_{\mathrm{APC}}| \tag{20}$$

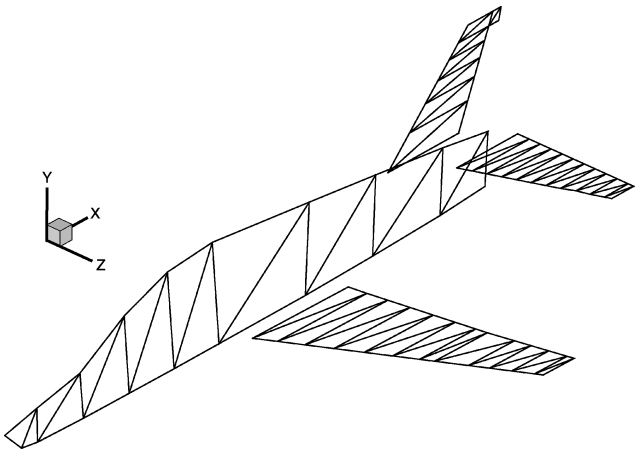

Fig. 3 Triangular surface elements for a structural model of the Hawk.

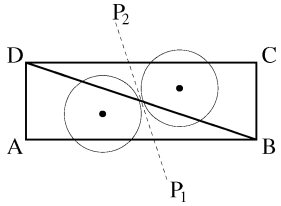

Fig. 4 Search domains when using the triangle centroids to map fluid points onto triangles.

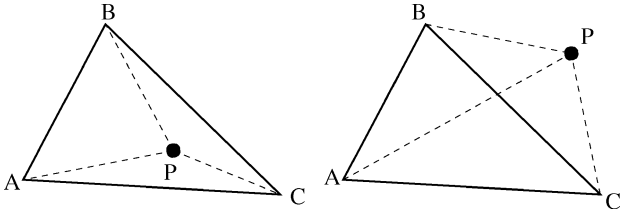

Fig. 5 Search cases when placing projected points into triangles.

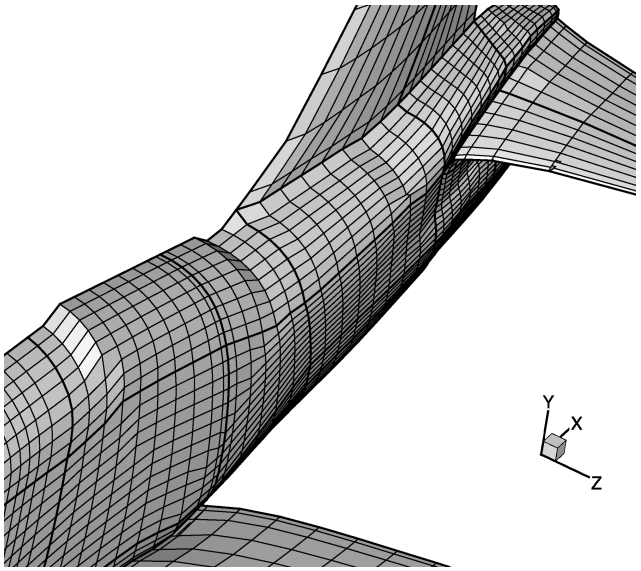

a) Nearest centroid

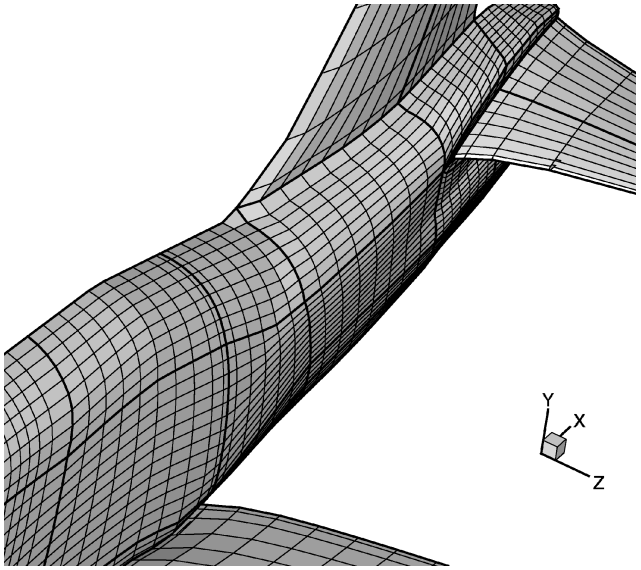

b) Areas

Fig. 6 Difference in the transformed surface as a result of search method used.

The minimization of $X_{\triangle_j}$ is used to associate $\triangle_i$ to point $\boldsymbol{x}_{f,i}$, and because $X_{\triangle_j}$ is zero if the projected point is inside the triangle this also minimizes the number of displacements calculated using extrapolation.

Figure 6 shows the difference between the two methods of association when used to transform one of the structural modes. The fuselage is smoother using the new scheme.

Results

The simulation method just described is demonstrated for the Hawk aircraft in level flight, zero angle of attack, and through the transonic flow regime. Some simplifications to the Hawk geometry have been made to reduce the complexity of the CFD grid-generation task. This is in common with other complete aircraft demonstrations where various combinations of the intake, vertical fin and tip missiles have been removed (see Melville,[10] Farhat et al.,[11] and Pranata et al.[12]). In the current case the wing-tip missiles and the intakes have been removed. In addition, linear analysis has shown that for this aircraft in this flight condition the symmetric modes are most unstable. It is the intention here to apply as rigorous an assessment of the results as is practically possible, and therefore the symmetric case is simulated to allow greater grid density to be used. However

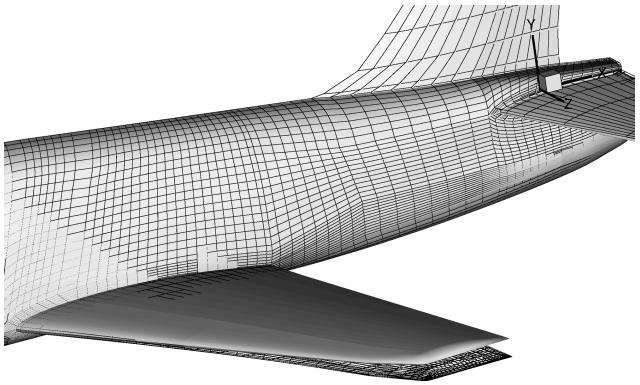

a) Bending mode

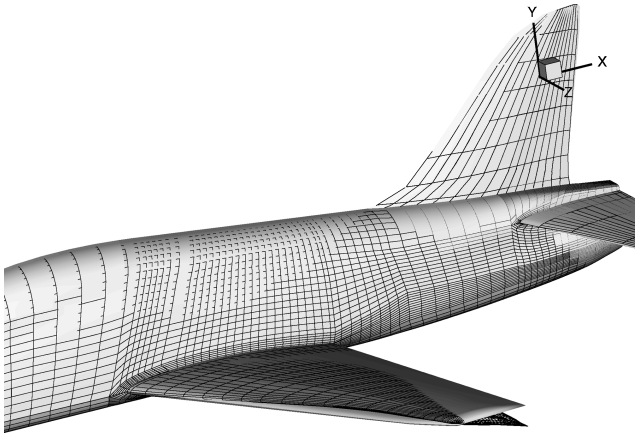

b) Torsion mode

Fig. 7 Transformation of wing-bending and torsion modes.

it is stressed that none of these simplifications are essential and all of these effects can be included as the codes stand, but with more effort on the grid generation or increased CPU time. In addition, no jet condition was applied at the back of the aircraft, and to avoid problems in predicting the aerodynamics in that region, particularly because we are using the Euler equations, a rigid sting was extended from the rear of the fuselage to the far field. This configuration is referred to as full.

The flutter mechanism turns out to be the interaction of wing bending and torsion modes. A simpler configuration was defined to allow a more detailed grid-refinement study. The wing only was retained for the CFD calculations with the full aircraft structural model used. This means that the wing is free to move at the root. The transformation of the wing bending and torsion modes is shown in Fig. 7.

The influence of the fuselage on the aerodynamics is not included for any of the linear results, and because we are dealing with the symmetric modes only the vertical fin makes no contribution to the aerodynamics in the full case. This is consistent with the usual practice.

Grid

For the full case a multiblock structured grid consisting of 141 blocks was constructed around the symmetric half of the aircraft using ICEMCFD. The far field is shaped as a bullet, which is 20 wing-root chords ahead of the nose and 19.5 chords behind the tail. The far field is 16 chords in diameter. An O-type blocking is used to grid the fuselage and C-H-type blocking to grid the wing and the elevator, that is, C-type around the rounded leading edges and H-type around the collapsed wing tips. The vertical fin is gridded with H-H-type blocking. The normal cell spacings on the wing and elevator surfaces are 10^{-3} chords. The fine volume grid has 4.45 million points. A medium grid is extracted from the fine grid by removing every alternate point in all three directions. A coarse grid is extracted from the medium grid in the same manner. The medium and coarse

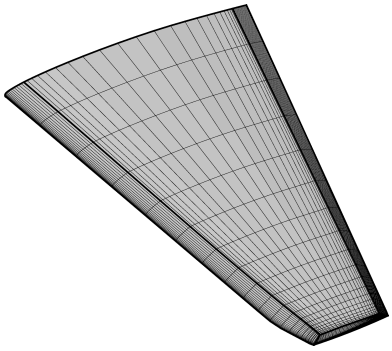

Fig. 8 Surface topology and grid for the wing-only configurations.

volume grids have 610,000 and 91,000 points respectively, and the respective grids have 14,000 and 3500 points on the surface of the aircraft. The grid in Farhat et al.[11] has 403,000 vertices for an Euler calculation around the full F-16 (but without the wing-tip missiles). Melville[10] uses 1.7 million points for the full F-16 RANS calculations, including the wing-tip missiles but excluding the intake. These grids are likely to be comparable in density to the medium grid defined here.

It was established from the linear and full CFD results that the flutter mechanism is a wing bending-torsion interaction. The C-H topology around the wing in the full grid is not very efficient at resolving this sort of problem because the important contribution from the aerodynamics comes from the vicinity of the wing tip, and this grid topology does not concentrate points easily in this region. A grid-independent solution on the full grids was not obtained. Therefore a second series of grids, which have an O-O topology, was generated. This was done for the wing configuration as experiments with the linear solutions suggested that the tailplane had only a marginal influence on the flutter behavior. The footprint of the blocks on the surface geometry is shown in Fig. 8 along with the surface grid itself. The block topology leads to a large number of points on the wing surface. It will be shown next that grid-independent solutions can be obtained on this family of grids. This sort of topology around the trailing edge is not good at preserving wakes, but the current calculations are inviscid so this is of no concern. For the wing-only grid, there are 845,000 points on the fine level, with 11,565 points on the wing surface. The medium and coarse levels have 114,000 and 166,000 points in the volume grid and 2919 and 744 points on the wing surface, respectively.

CFD Simulation

A grid sensitivity study based on steady flow was first performed to establish confidence in the resolution used for the full configuration. The surface plots of pressure coefficient for the rigid steady-state calculation are shown in Fig. 9. The shock over the upper surface of the wing is sharp and well defined on the fine grid but is a little smeared in the coarse. The coarse grid is however able to capture the location of the shock quite reasonably. Overall the results are remarkably similar between the three grid levels and suggest that the medium grid could be satisfactory for the aeroelastic calculations.

The behavior of the time response calculations however indicates otherwise. There was a significant difference between the coarse, medium, and fine predictions of flutter speed, with the medium grid predicting a value about 15% above the linear predictions, and the fine result indicating that this is down to grid resolution. Rather than pursuing a costly study on the fine grid, the wing-only configuration was used in the expectation that 1) the concentration of points in the wing-tip region would allow a grid-converged solution to be obtained and 2) this could represent the flutter mechanism. The surface plots of pressure coefficient on the medium grid for the wing-only case is also indicated in Fig. 9 and shows good agreement for the steady test case. Flutter speed predictions on the different grid levels are shown next.

All of the calculations were run on a cluster of 2.5-GHz PCs running under Linux and connected by 100-Mbit Fast Ethernet. The

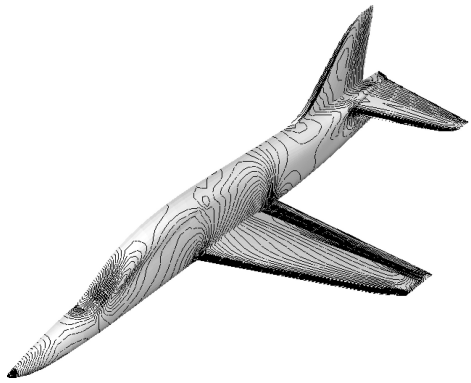

a) Surface *Cp* contours on the full coarse grid

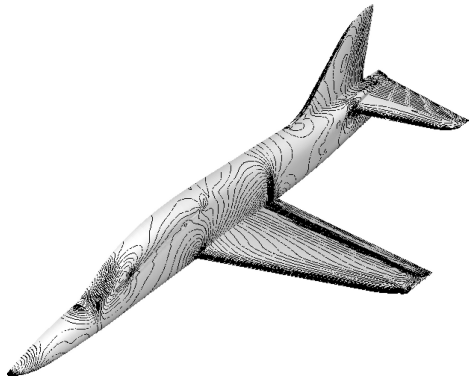

b) Surface *Cp* contours on the full medium grid

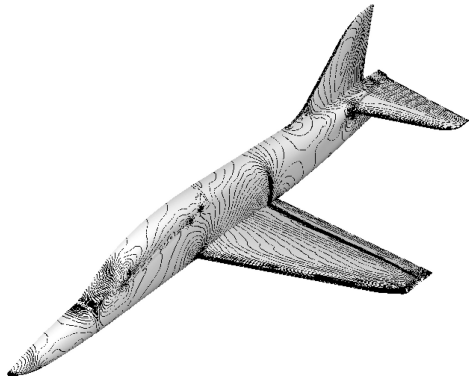

c) Surface *Cp* contours on the full fine grid

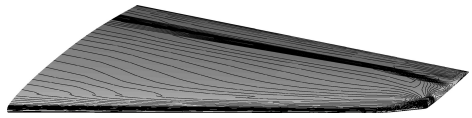

d) Surface *Cp* contours on the wing only medium grid

Fig. 9 Surface *Cp* contours for a steady rigid transonic case.

CFD group at Glasgow has a cluster of 72 machines, and this represents a powerful and affordable system. For the full medium grid, driving the residual down six orders on eight processors, the calculation required 35 min. Solving on the coarse grid on one processor, a final convergence of eight orders required 22 min. For the wing only the times were 44 s, 35 min, and 60 min on one, one, and eight processors for the coarse, medium, and fine levels, respectively.

Coupled CFD/CSD Simulation

Dynamic calculations were then carried out. A rigid steady-state calculation was used to initialise a static aeroelastic calculation, which in fact converged rapidly because a very small deformation was observed. Then, a nonzero generalized velocity for the first mode was set, and the time-marching calculations started. The

response for different values of dynamic pressure was obtained, and the airspeed at which stability is lost was inferred from the growth or decay of these responses. The linear results suggested that the flutter speed is insensitive to the value of structural damping, and a value of 0% was used in the CFD calculations.

A detailed time-step convergence study was carried out for all three configurations, and negligible differences between using 50 time steps per flutter cycle and smaller time steps were observed on all grids and at all Mach numbers. Hence, this time step was used.

As just stated, the full configuration grids were found to give dynamic behavior that is too damped. This is ascribed to a lack of resolution in the crucial wing-tip region. The flutter speed was bracketed at a series of freestream Mach numbers on the wing-only grids, and the results are compared in Fig. 10 with the linear results for the full configuration. First, the wing-only results show convergence between the results on the medium and fine grids, at both a low subsonic and a transonic freestream Mach number.

The medium grid and linear results are in close agreement for all Mach numbers below a supersonic freestream, when the CFD-generated results show a significant rise in the flutter speed as the shock wave reaches the trailing edge. In this case there is no evidence of a significant flutter dip, perhaps because the Hawk structure is extremely rigid. To test this, the structural model was weakened by reducing the elastic modulus by an order of magnitude. The comparison between the linear and CFD predictions for the wing-only configuration on the medium grid is shown in Fig. 11. In this case the CFD-generated speeds dip below the linear predictions in the transonic range.

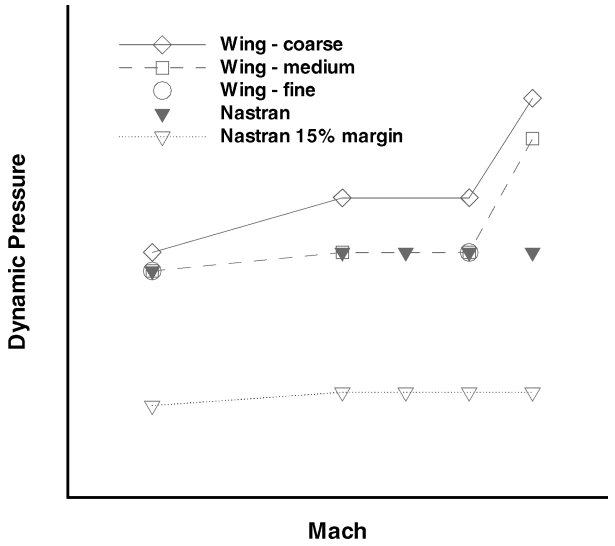

Fig. 10 Comparison between the flutter boundaries predicted using the linear method and the wing-only configurations.

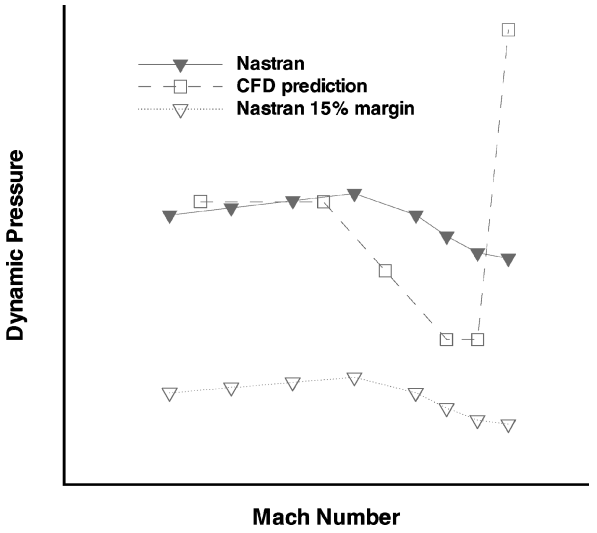

Fig. 11 Comparison between the flutter boundaries predicted using the linear method and the wing-only configuration for the weakened structural model.

Again the full configuration coarse grid calculations were run on a single processor and the medium ones on eight processors. A tight convergence criterion criteria was adopted, and the calculations were run forward for 1600 real steps. The coarse grid calculations (with a tighter convergence criterion) required 12 h and the medium grid calculations 7 h. For the wing-only grid, the times were 1 h on a single processor, 9 h on one processor, 16 h on eight processors on the coarse, medium, and fine grids, respectively.

Conclusions

Time-marching computational-fluid-dynamics (CFD)-based aeroelastic calculations for the Hawk aircraft have been demonstrated. A structural model developed by BAE Systems, and appropriate for linear flutter calculations, was used, and the coarseness of this model posed problems for the transfer of information to the fluid grid. Various elements of the transformation method, including how the fluid points are mapped to the structural elements, and how the different components are tied together, were reconsidered to meet the challenges posed by the complete aircraft.

Flutter calculations were run on a sequence of grids for two configurations, first retaining the wing-body-fin-tailplane and then the wing only. This allowed a detailed grid-refinement study. It was found that the flutter mechanism was wing-bending torsion interaction and that a grid-converged solution was obtained with a reasonable number of grid points if a suitable block topology was used. No flutter dip was seen for the real aircraft structural model, possibly because the aircraft is so structurally rigid, but a weakended version of the model showed a transonic dip when using the CFD.

The calculations here did not require expensive computer resources. The worst case would allow two calculations on the full configuration medium grid to be run overnight using eight modern PC nodes. This level of performance demonstrates the feasibility of exploiting this capability for routine nonlinear flutter prediction.

The next stage of this work is to evaluate potentially more realistic flutter problems, which are usually associated with attachments to the wing such as missiles, tanks, or control surfaces. The work described in this paper provides the opportunity to progress with this.

Acknowledgments

This work was supported by BAE SYSTEMS, Engineering and Physical Sciences Research Council and Ministry of Defence and is part of the work programme of the Partnership for Unsteady Methods in Aerodynamics Defence and Aerospace Research Partnership. The authors gratefully acknowledge the help of Alan Sowden of BAE Systems for providing the structural model and for general advice on linear methods.

References

[1]Tsai, H. M., Wong, A. S. F., Cai, J., Zhu, Y., and Liu, F., "Unsteady Flow Calculations with a Parallel Multiblock Moving Mesh Algorithm," *AIAA Journal*, Vol. 39, No. 6, 2001, pp. 1021–1029.

[2]Rausch, R. D., Batina, J. T., and Yang, H. T., "Three-Dimensional Time-Marching Aeroelastic Analyses Using an Unstructured-Grid Euler Method," *AIAA Journal*, Vol. 31, No. 9, 1993, pp. 1626–1633.

[3]Lesoinne, M., and Farhat, C., "Geometric Conservation Laws for Flow Problems with Moving Boundaries and Deformable Meshes and Their Impact on Aeroelastic Computations," *Computer Methods in Applied Mechanics and Engineering*, Vol. 134, 1996, pp. 71–90.

[4]Farhat, C., and Lesoinne, M., "Two Efficient Staggered Procedures for the Serial and Parallel Solution of Three-Dimensional Nonlinear Transient Aeroelastic Problems," *Computer Methods in Applied Mechanics and Engineering*, Vol. 182, 2000, pp. 499–516.

[5]Brown, S. A., "Displacement Extrapolation for CFD and CSM Aeroelastic Analysis," AIAA Paper 97-1090, April 1997.

[6]Goura, G. S. L., Badcock, K. J., Woodgate, M. A., and Richards, B. E., "A Data-Exchange Method for Fluid-Structure Interaction Problems," *Aeronautical Journal*, No. 1046, April 2001, pp. 215–222.

[7]Smith, M. J., Hodges, D. H., and Cesnik, C. E. S., "Evaluation of Computational Algorithms Suitable for Fluid-Structure Interactions," *Journal of Aircraft*, Vol. 37, No. 2, 2000, pp. 282–294.

[8]Goura, G. S. L., Badcock, K. J., Woodgate, M. A., and Richards, B. E., "Extrapolation Effects on Coupled Computational Fluid Dynamics/Computational Structural Dynamics Simulations," *AIAA Journal*, Vol. 41, No. 2, 2003, pp. 312–314.

[9]Dreim, D. R., Jacobsen, S. B., and Britt, R. T., "Simulation of Non-Linear Transonic Aeroelastic Behaviour on the B2," *Proceedings of International Forum on Aeroelasticity and Structural Dynamics*, edited by W. Whitlow and E. Todd, NASA Langley, Hampton, VA, 1999, pp. 511–522.

[10]Melville, R., "Nonlinear Simulation of F-16 Aeroelastic Instability," AIAA Paper 2001-0570, Jan. 2001.

[11]Farhat, C., Geuzaine, P., and Brown, G., "Application of a Three-Field Nonlinear Fluid-Structure Formulation to the Prediction of the Aeroelastic Parameters of an F-16 Fighter," *Computers and Fluids*, Vol. 32, No. 3, 2002, pp. 3–29.

[12]Pranata, B. B., Kok, J. C., Spekreijse, S. P., Hounjet, M. H. L., and Meijer, J. J., "Simulation of Limit Cycle Oscillation of Fighter Aircraft at Moderate Angle of Attack," *Proceedings of International Forum on Aeroelasticity and Structural Dynamics*, edited by W. Whitlow and E. Todd, NASA Langley, Hampton, VA, 1999, pp. 511–522.

[13]Goura, G. S. L., "Time Marching Analysis of Flutter Using Computational Fluid Dynamics," Ph.D. Dissertation, Dept. of Aerospace Engineering, Univ. of Glasgow, Scotland, U.K., Sept. 2001.

[14]Badcock, K. J., Rampurawala, A. M., and Richards, B. E., "An Assessment of Inter-Grid Transformation for a Whole Aircraft," *AIAA Journal*, Vol. 42, No. 9, 2004, pp. 1936–1939.

[15]Osher, S., and Chakravarthy, S., "Upwind Schemes and Boundary Conditions with Applications to Euler Equations in General Geometries," *Journal of Computational Physics*, Vol. 50, 1983, pp. 447–481.

[16]Van Leer, B., "Towards the Ultimate Conservative Difference Scheme II: Monotonicity and Conservation Combined in a Second Order Scheme," *Journal of Computational Physics*, Vol. 14, 1974, pp. 361–374.

[17]Jameson, A., "Time Dependent Calculations Using Multigrid, with Applications to Unsteady Flows past Airfoils and Wings," AIAA Paper 91-1596, 1991.

[18]Gordon, W. J., and Hall, C. A., "Construction of Curvilinear Coordinate Systems and Applications to Mesh Generation," *International Journal for Numerical Methods in Engineering*, Vol. 7, 1973, pp. 461–477.

[19]Badcock, K. J., Richards, B. E., and Woodgate, M. A., "Elements of Computational Fluid Dynamics on Block Structured Grids Using Implicit Solvers," *Progress in Aerospace Sciences*, Vol. 36, 2000, pp. 351–392.

[20]Goura, G. S. L., Badcock, K. J., Woodgate, M. A., and Richards, B. E., "Implicit Method for the Time Marching Analysis of Flutter," *Aeronautical Journal*, Vol. 105, No. 1046, April 2001, pp. 199–214.

[21]Lucia, D., Beran, P. S., and Silva, W., "Aeroelastic System Development Using Proper Orthogonal Decomposition and Volterra Theory," AIAA Paper 2003-1922, 2003.